

All-optical injection of charge, spin, and valley currents in monolayer transition-metal dichalcogenides

Rodrigo A. Muniz and J. E. Sipe

Department of Physics and Institute for Optical Sciences, University of Toronto, Toronto, Ontario M5S 1A7, Canada

(Received 10 September 2014; revised manuscript received 8 January 2015; published 5 February 2015)

Monolayer transition-metal dichalcogenides have recently become a playground for spintronics and valleytronics research. Their low-energy spectrum can be described by Dirac cones on the corners of Brillouin zone, but the physical properties are richer than those of graphene since the spin degeneracy is lifted and the optical selection rules are valley dependent. This has been exploited for the optical injection of spin- and valley-polarized currents by the application of static electric fields. In this paper we consider an all-optical method for the injection of charge-, spin-, and valley-polarized currents. The presence of both a fundamental optical field and its second harmonic can lead to the injection of currents due to a nonlinear effect involving the quantum interference between one- and two-photon absorption processes. We analyze how the injected quantities can be controlled through the parameters of the incident light fields, allowing capabilities of control beyond those achieved with static fields, and discuss the conditions for experimental verification of our results.

DOI: [10.1103/PhysRevB.91.085404](https://doi.org/10.1103/PhysRevB.91.085404)

PACS number(s): 73.20.-r, 72.25.Fe, 42.65.-k, 78.20.-e

I. INTRODUCTION

The optoelectronic properties of two-dimensional materials are often qualitatively different from those of their three-dimensional counterparts. Novel fields of research that arise from these differences, such as valleytronics [1], hold promise for the development of new technologies. In addition, these materials can be conspicuously integrated into heterostructures, as coatings for example, paving the way for their application in integrated optical devices. An outstanding class of two-dimensional materials are the monolayer transition-metal dichalcogenides (TMD), which have recently been shown to display several interesting electronic and optical properties [2,3]. Their atomic structure consists of a hexagonal lattice, and the low-energy spectrum is described by gapped Dirac cones on the corners of the Brillouin zone. Due to strong spin-orbit coupling and broken inversion symmetry, the spin degeneracy is lifted in opposite ways in the two valleys, and the optical selection rules are valley dependent [4,5]. Therefore, according to the helicity of incident light, optically excited carriers are valley polarized and, for low enough photon energies, also spin polarized [6–8]. The injected carriers can be then driven by an electric field, providing a valley and spin polarized current [9–11]. Such currents have been the subject of intensive research, with respect to both fundamental questions and technological applications [2].

Even though some nonlinear optical properties of monolayer TMDs have been studied [12,13], the proposals for current injection have so far focused on the application of static fields. However, the need of a static applied electric field does not allow for fast switching, and offers only limited control of the currents. In order to better understand these materials, it would be desirable to have an all-optical method for the injection of currents, since it would allow for faster switching and more refined control over the quantities of interest by using, for example, the polarizations and phase parameters of the incident fields. This would allow for a more detailed analysis of optoelectronic properties of monolayer TMDs.

Effective all-optical injection of currents can be achieved by coherent control. It makes use of both a fundamental

optical field and its second harmonic, which allows for optical injection of currents by a nonlinear process involving quantum interference between one- and two-photon absorption [14]. It has been applied in several experimental scenarios involving bulk and nanostructure semiconductors [14–19,28], it has been predicted and seen in graphene [20–22], and experiments to lead to its observation in topological insulators have recently been proposed [23]. Here we study how it can be used for the injection of polarized currents in monolayer TMDs. We compute the optical injection rates of several quantities for monolayer films of TMDs. The quantities considered are carrier, spin, and valley polarization densities, as well as charge, spin, and valley currents. We show how the polarization and a relative phase parameter of the incident fields can be used to control the optical generation of quasiparticles and their currents on time scales set by the duration of laser pulses.

This article is organized in the following form: in Sec. II we present the model for monolayer TMDs used for our calculations. Section III contains an outline of the computation for the optical injection rate coefficients corresponding to carrier, spin, and valley densities, as well as charge, spin, and valley currents. In Sec. IV we show the results obtained for different polarizations and relative orientations of the incident fields. The explicit expression for the injection rate coefficients are shown in the Appendix A. We conclude with a discussion about the experimental verification of our results in Sec. V. Since the experimental techniques required to confirm our results are well established, we expect that such experiments will help advance the understanding and applications of optically injected currents in monolayer TMDs.

II. MODEL FOR MONOLAYERS OF TRANSITION-METAL DICHALCOGENIDES

The calculation of injection rates is performed using Fermi's golden rule in a method described earlier [23], where general expressions were provided for a two-band Hamiltonian. The main steps of the calculation are provided in the next section. Here we focus on the particular model

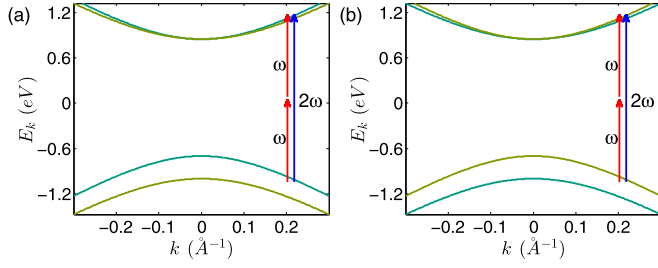


FIG. 1. (Color online) Bands at the two valleys with the absorption processes indicated. (a) $\tau = 1$, and (b) $\tau = -1$. Different colors of the bands distinguish between spin (\uparrow green) and (\downarrow yellow). Note that bands with the same energy have opposite spins on the two different valleys.

used to describe monolayer TMDs. The main information about the model necessary for carrying out the calculations is the matrix elements of the velocity operator, since the external perturbative Hamiltonian depends on it, as well as the difference between the conduction and valence matrix elements of the operators associated with the quantities that are injected. However, the velocity operator is the only nontrivial operator needed, as the operators corresponding to the quantities we consider are related to it. So our goal in this section is to obtain expressions for those matrix elements.

The simplest model for TMDs has a four-band Hamiltonian with two valleys, totaling eight states for each small lattice momentum \mathbf{k} around the corners of the Brillouin zone. For each valley, K ($\tau = +1$) and K' ($\tau = -1$), and each spin, \uparrow ($s = 1$) and \downarrow ($s = -1$), the model leads to a gapped Dirac cone described by the matrix [4,5]

$$H_{\tau,s,k} = \hbar t(\tau k_x \sigma_x + k_y \sigma_y) + \frac{\hbar \Delta}{2} \sigma_z + \frac{\hbar \lambda \tau s}{2} (\sigma_0 - \sigma_z), \quad (1)$$

where Δ and λ are parameters with dimensions of frequency, t is another parameter with dimension of velocity. The parameters used in the calculations for the figures in this paper correspond to those of MoS₂ and are listed later in Table I, in Sec. IV, where we show our results. For a given τ and s , (1) the generic form of a two-band system Hamiltonian

$$H_k = \hbar \varpi_k \sigma_0 + \hbar \mathbf{d}_k \cdot \boldsymbol{\sigma}, \quad (2)$$

with

$$\begin{aligned} \varpi_k &= \frac{\lambda \tau s}{2}, \\ \mathbf{d}_k &= t \tau k_x \hat{\mathbf{x}} + t k_y \hat{\mathbf{y}} + \Delta_{\tau s} \hat{\mathbf{z}}, \end{aligned} \quad (3)$$

where $\Delta_{\tau s} = (\Delta - \lambda \tau s)/2$.

In agreement with earlier notation [23], the eigenenergies for Eq. (2) are written as $E_{k\pm} = \hbar(\varpi_k \pm d_k)$ where $d_k = |\mathbf{d}_k|$, with (+) = c and (−) = v representing the conduction and valence bands respectively; we also denote $\omega_{cv,k} \equiv \hbar^{-1}(E_{k,c} - E_{k,v}) = 2d_k$. The energy bands for each valley are displayed in Fig. 1; notice the opposite spin splitting for the two valleys. The Hamiltonian is diagonalized by the unitary matrix $U_k = \exp(-i\frac{\phi_k}{2}\hat{\mathbf{n}}_k \cdot \boldsymbol{\sigma})$, with $\hat{\mathbf{n}}_k = \hat{\mathbf{z}} \times \hat{\mathbf{d}}_k/|\hat{\mathbf{z}} \times \hat{\mathbf{d}}_k|$ and $\cos \phi_k = \hat{\mathbf{z}} \cdot \hat{\mathbf{d}}_k$. In order to write arbitrary operators in the basis of eigenstates, it is useful to consider the triad $\Xi = \{\hat{\mathbf{n}}_k, \hat{\mathbf{d}}_k, \hat{\mathbf{n}}_k \times \hat{\mathbf{d}}_k\}$, which forms an orthonormal basis.

Additionally, since it is known how the operators associated to each vector in Ξ are expressed in the basis of eigenstates, an arbitrary operator $\hat{\mathbf{w}} \cdot \boldsymbol{\sigma}$ can be easily written in the basis of eigenstates $U_k^\dagger (\hat{\mathbf{w}} \cdot \boldsymbol{\sigma}) U_k$ by decomposing $\hat{\mathbf{w}}$ in the triad Ξ .

The velocity operator $v_k^a = \hbar^{-1} \partial_{k^a} H_k$ plays a fundamental role in the determination of optical properties. For a generic two-band model described by the Hamiltonian (2), written in the basis of eigenstates, v_k^a is given by

$$\begin{aligned} v_k^a &= \partial_{k^a} \varpi_k \sigma_0 + \partial_{k^a} d_k \sigma_z + d_k (\hat{\mathbf{n}}_k \cdot \partial_{k^a} \hat{\mathbf{d}}_k) \hat{\mathbf{n}}_k \cdot \boldsymbol{\sigma} \\ &+ d_k [(\hat{\mathbf{n}}_k \times \hat{\mathbf{d}}_k) \cdot \partial_{k^a} \hat{\mathbf{d}}_k] (\hat{\mathbf{n}}_k \times \hat{\mathbf{z}}) \cdot \boldsymbol{\sigma}. \end{aligned} \quad (4)$$

As it will be clear in Sec. III, the specific matrix elements necessary for the calculation of the injection rates are

$$\begin{aligned} v_{cc}^a - v_{vv}^a &= 2\partial_{k^a} d_k, \\ v_{cv}^a v_{vc}^b &= d_k^2 [\partial_{k^a} \hat{\mathbf{d}}_k \cdot \partial_{k^b} \hat{\mathbf{d}}_k + i \hat{\mathbf{d}}_k \cdot (\partial_{k^a} \hat{\mathbf{d}}_k \times \partial_{k^b} \hat{\mathbf{d}}_k)]. \end{aligned} \quad (5)$$

For the system under consideration, $\hat{\mathbf{n}}_k = \frac{1}{k}(-k_y \hat{\mathbf{x}} + \tau k_x \hat{\mathbf{y}})$ and $d_k = \sqrt{t^2 k^2 + \Delta_{\tau s}^2}$, so

$$\begin{aligned} \partial_{k^b} d_k &= \frac{t^2 k^b}{d_k}, \\ \partial_{k^b} \hat{\mathbf{d}}_k &= \frac{t(\tau b^x \hat{\mathbf{x}} + b^y \hat{\mathbf{y}})}{d_k} - \frac{t^2 k^b \mathbf{d}_k}{d_k^3}, \end{aligned} \quad (6)$$

and

$$\begin{aligned} \partial_{k^a} \hat{\mathbf{d}}_k \cdot \partial_{k^b} \hat{\mathbf{d}}_k &= \frac{t^2 \hat{\mathbf{a}} \cdot \hat{\mathbf{b}}}{d_k^2} - \frac{2t^4 k^a k^b}{d_k^4} + \frac{t^4 k^a k^b}{d_k^4} \\ &= \frac{t^2 \hat{\mathbf{a}} \cdot \hat{\mathbf{b}}}{d_k^2} - \frac{t^4 k^a k^b}{d_k^4}, \\ \hat{\mathbf{d}}_k \cdot (\partial_{k^a} \hat{\mathbf{d}}_k \times \partial_{k^b} \hat{\mathbf{d}}_k) &= \frac{t^2 \tau \mathbf{d}_k \cdot (\hat{\mathbf{a}} \times \hat{\mathbf{b}})}{d_k^3} = \frac{t^2 \tau \Delta_{\tau s} \hat{\mathbf{z}} \cdot (\hat{\mathbf{a}} \times \hat{\mathbf{b}})}{d_k^3}, \end{aligned} \quad (7)$$

which then gives

$$\begin{aligned} v_{cc}^a - v_{vv}^a &= \frac{2t^2 k^a}{d_k}, \\ v_{cv}^a v_{vc}^b &= t^2 \left[\hat{\mathbf{a}} \cdot \hat{\mathbf{b}} - \frac{t^2 k^a k^b}{d_k^2} + i \frac{\tau \Delta_{\tau s} \hat{\mathbf{z}} \cdot (\hat{\mathbf{a}} \times \hat{\mathbf{b}})}{d_k} \right]. \end{aligned} \quad (8)$$

The last term in the expressions for $v_{cv}^a v_{vc}^b$ is related to the chirality χ of the Dirac cone

$$\chi_{\tau s} = t^{-2} d_k^2 \hat{\mathbf{d}}_k \cdot (\partial_{k^x} \hat{\mathbf{d}}_k \times \partial_{k^y} \hat{\mathbf{d}}_k) \Big|_{k=0} = \tau \frac{\Delta_{\tau s}}{|\Delta_{\tau s}|}, \quad (9)$$

which is signaled by the opposite signs of the Berry curvature of the corresponding valence ($F_{\tau s, v}$) and conduction ($F_{\tau s, c} = -F_{\tau s, v}$) bands, which are

$$F_{\tau s, v} = \frac{1}{2} \hat{\mathbf{d}}_k \cdot (\partial_{k^x} \hat{\mathbf{d}}_k \times \partial_{k^y} \hat{\mathbf{d}}_k) = \tau \frac{t^2 \Delta_{\tau s}}{2(t^2 k^2 + \Delta_{\tau s}^2)^{\frac{3}{2}}}. \quad (10)$$

Optical properties of the system contain information of the Berry curvature and consequently the chirality of the excited

states. Indeed, the chirality of the Dirac cone has a strong effect on the optical selection rules for circularly polarized light, which is absorbed only by Dirac cones with a chirality that matches the helicity of the incident light. This is one of the reasons why the optical properties of TMDs are so interesting, as it will be seen in our results in Sec. IV.

Operators. The quantities of interest are the densities of carriers $\langle n \rangle$, spin $\langle S^z \rangle$ and valley $\langle \tau \rangle$ polarizations, as well as current densities of charge $\langle \mathbf{J}^c \rangle$, spin $\langle \mathbf{J}^s \rangle$, and valley $\langle \mathbf{J}^\tau \rangle$, whose conduction and valence matrix elements are shown below. We use the area density of all quantities, and in our calculations the inverse of area dimension arises in the integrals over the Brillouin zone necessary to obtain the expectation values. Thus in this notation \mathbf{J}_c has units of *charge* \times *velocity* while $\langle \mathbf{J}_c \rangle$ has units of *charge* \times *velocity*/*area*, for example.

We keep track of the injected carriers by computing the density of electrons injected into the conduction band. For each Dirac cone (labeled by the indices s and τ), the corresponding number operator has matrix elements $n_{cc} = 1$ and $n_{vv} = 0$, for all the four Dirac cones. The operators corresponding to polarizations of spin $S^z = \frac{\hbar}{2}s\sigma_z$ and valley $\mathcal{T} = \tau\sigma_z$ have matrix elements $S_{cc}^z = \frac{\hbar}{2}s$ and $S_{vv}^z = -\frac{\hbar}{2}s$, and $\tau_{cc} = \tau$ and $\tau_{vv} = -\tau$, for each Dirac cone.

The operators corresponding to currents of charge $\mathbf{J}^c = e\mathbf{v}$, spin $\mathbf{J}^s = \frac{\hbar}{2}s\mathbf{v}$, and valley $\mathbf{J}^\tau = \tau\mathbf{v}$, are expressed in terms of the velocity operator \mathbf{v} .

Summarizing, we have

$$\begin{aligned} n_{cc} - n_{vv} &= 1, \\ S_{cc}^z - S_{vv}^z &= \hbar s, \\ \tau_{cc} - \tau_{vv} &= 2\tau, \end{aligned} \quad (11)$$

for carriers number, spin, and valley, and

$$\begin{aligned} \mathbf{J}_{cc}^c - \mathbf{J}_{vv}^c &= e(\mathbf{v}_{cc} - \mathbf{v}_{vv}), \\ \mathbf{J}_{cc}^s - \mathbf{J}_{vv}^s &= \frac{\hbar}{2}s(\mathbf{v}_{cc} - \mathbf{v}_{vv}), \\ \mathbf{J}_{cc}^\tau - \mathbf{J}_{vv}^\tau &= \tau(\mathbf{v}_{cc} - \mathbf{v}_{vv}), \end{aligned} \quad (12)$$

for the charge, spin, and valley currents.

III. OPTICAL INJECTION RATES

As mentioned before, the calculation for the injection rates is carried out using Fermi's golden rule, since it makes evident

all the contributions stemming from one- and two-photon processes and their interference; this is a feature not shared by the Kubo formalism, for instance. The general formulation has been already well explained in previous studies [14,23], so we only show the information that is specific for monolayer TMDs.

The incident light is described by the electric field $\mathbf{E}(t) = \sum_n \mathbf{E}(\omega_n) e^{-i\omega_n t}$, with $\omega_n = \pm\omega, \pm 2\omega$. It corresponds to the interaction Hamiltonian $V_{ext} = ie \sum_n \mathbf{v} \cdot \mathbf{E}(\omega_n) e^{-i\omega_n t} / \omega_n$, which is treated perturbatively within the Fermi's golden rule formalism; $e = -|e|$ is the electron charge. The injection rate will have a first-order term proportional to V_{ext}^2 , a second-order one proportional to V_{ext}^4 , and so on. There will also be an interference term between the first and second order, which is proportional to V_{ext}^3 . The injection rate for the density $\langle M \rangle$ of a quantity associated with a single-particle operator $\mathcal{M} = \sum_{\mathbf{k}} a_{\alpha,\mathbf{k}}^\dagger M_{\alpha\beta,\mathbf{k}} a_{\beta,\mathbf{k}}$, where α and β are band indices. $\langle M \rangle$ can be decomposed into contributions from one- and two-photon absorption processes together with their interference term, $\langle \dot{M} \rangle = \langle \dot{M}_1 \rangle + \langle \dot{M}_2 \rangle + \langle \dot{M}_i \rangle$ where

$$\begin{aligned} \langle \dot{M}_1 \rangle &= \sum_{n=1,2} \Lambda_1^{bc}(n\omega) E^b(-n\omega) E^c(n\omega), \\ \langle \dot{M}_2 \rangle &= \Lambda_2^{bcde}(\omega) E^b(-\omega) E^c(-\omega) E^d(\omega) E^e(\omega), \\ \langle \dot{M}_i \rangle &= \Lambda_i^{bcd}(\omega) E^b(-\omega) E^c(-\omega) E^d(2\omega) + cc. \end{aligned} \quad (13)$$

The optical injection coefficients Λ associated with \mathcal{M} are obtained from integrals over the Brillouin zone; if \mathbf{k} is represented in polar coordinates, the integral over the radial component enforces the energy matching condition ($\omega_{cv} = \omega$ or $\omega_{cv} = 2\omega$), and only the angular integral remains [23],

$$\begin{aligned} \Lambda_1^{bc}(\omega) &= \int \frac{d\theta}{2\pi} \frac{d_{\mathbf{k}}(M_{cc,\mathbf{k}} - M_{vv,\mathbf{k}}) \Gamma_{1,cv}^{bc}(\mathbf{k}, \omega)}{2t^2} \Big|_{d_{\mathbf{k}}=\frac{\omega}{2}}, \\ \Lambda_2^{bcde}(\omega) &= \int \frac{d\theta}{2\pi} \frac{d_{\mathbf{k}}(M_{cc,\mathbf{k}} - M_{vv,\mathbf{k}}) \Gamma_{2,cv}^{bcde}(\mathbf{k}, \omega)}{2t^2} \Big|_{d_{\mathbf{k}}=\omega}, \\ \Lambda_i^{bcd}(\omega) &= \int \frac{d\theta}{2\pi} \frac{d_{\mathbf{k}}(M_{cc,\mathbf{k}} - M_{vv,\mathbf{k}}) \Gamma_{i,cv}^{bcd}(\mathbf{k}, \omega)}{2t^2} \Big|_{d_{\mathbf{k}}=\omega}, \end{aligned} \quad (14)$$

where

$$\begin{aligned} \Gamma_{1,cv}^{bc}(\mathbf{k}, \omega) &= \frac{e^2 v_{cv}^c v_{vc}^b}{\hbar^2 \omega^2}, \\ \Gamma_{2,cv}^{bcde}(\mathbf{k}, \omega) &= \frac{e^4 t^4}{\hbar^4 \omega^6} \left[\frac{k^c k^e v_{cv}^d v_{vc}^b + k^c k^d v_{cv}^e v_{vc}^b + k^b k^e v_{cv}^d v_{vc}^c + k^b k^d v_{cv}^e v_{vc}^c}{d_{\mathbf{k}}^2} \right], \\ \Gamma_{i,cv}^{bcd}(\mathbf{k}, \omega) &= \frac{ie^3 t^2}{2\hbar^3 \omega^4} \left[\frac{k^c v_{cv}^d v_{vc}^b + k^b v_{cv}^d v_{vc}^c}{d_{\mathbf{k}}} \right], \end{aligned} \quad (15)$$

and the integrals are over the circle in the Brillouin zone set by the energy matching condition $\omega_{cv} = \omega$ or $\omega_{cv} = 2\omega$.

Optical injection coefficients. We now look at the injection coefficients Λ_N ($N = 1, 2, i$) associated with the injection densities $\langle M \rangle$ for our quantities of interest. For the densities of carriers $\langle n \rangle$, spin $\langle S^z \rangle$, and valley $\langle \tau \rangle$, we denote the optical injection coefficients by ξ_N , ζ_N and ϑ_N respectively, while for the densities of their corresponding currents of charge $\langle \mathbf{J}^c \rangle$, spin $\langle \mathbf{J}^s \rangle$, and valley $\langle \mathbf{J}^T \rangle$, we denote the optical injection coefficients by η_N , μ_N , and ν_N .

The expressions for the various optical injection coefficients are sums over the contributions from each of the four Dirac cones. After the integrals in Eq. (14) are evaluated with

the use of Eq. (8), we find three independent terms, namely $\xi_{1,\tau s}^{bc}$, $\xi_{2,\tau s}^{bcde}$, and $\eta_{i,\tau s}^{abcd}$, which are associated with carrier density and the charge current density respectively. They can be broken down into their chiral and nonchiral parts as

$$\begin{aligned}\xi_{1,\tau s}^{bc}(\omega) &= \bar{\xi}_{1,\tau s}^{bc}(\omega) + i\tau \tilde{\xi}_{1,\tau s}^{bc}(\omega), \\ \xi_{2,\tau s}^{bcde}(\omega) &= \bar{\xi}_{2,\tau s}^{bcde}(\omega) + i\tau \tilde{\xi}_{2,\tau s}^{bcde}(\omega), \\ \eta_{i,\tau s}^{abcd}(\omega) &= \bar{\eta}_{i,\tau s}^{abcd}(\omega) + i\tau \tilde{\eta}_{i,\tau s}^{abcd}(\omega),\end{aligned}\quad (16)$$

where

$$\begin{aligned}\bar{\xi}_{1,\tau s}^{bc}(\omega) &= \frac{\Theta(\omega - 2\Delta_{\tau s})e^2}{2\hbar^2\omega} \left(1 + \frac{4\Delta_{\tau s}^2}{\omega^2}\right) \frac{\hat{\mathbf{b}} \cdot \hat{\mathbf{c}}}{4}, \\ \bar{\xi}_{2,\tau s}^{bcde}(\omega) &= \frac{\Theta(\omega - \Delta_{\tau s})e^4 t^2}{\hbar^4\omega^5} \left(1 - \frac{\Delta_{\tau s}^2}{\omega^2}\right) \left[\left(1 + \frac{\Delta_{\tau s}^2}{\omega^2}\right) \frac{(\hat{\mathbf{b}} \cdot \hat{\mathbf{d}})\hat{\mathbf{c}} \cdot \hat{\mathbf{e}} + (\hat{\mathbf{b}} \cdot \hat{\mathbf{e}})\hat{\mathbf{c}} \cdot \hat{\mathbf{d}}}{4} - \left(1 - \frac{\Delta_{\tau s}^2}{\omega^2}\right) \frac{(\hat{\mathbf{b}} \cdot \hat{\mathbf{c}})\hat{\mathbf{d}} \cdot \hat{\mathbf{e}}}{4} \right], \\ \bar{\eta}_{i,\tau s}^{abcd}(\omega) &= \frac{i\Theta(\omega - \Delta_{\tau s})e^4 t^2}{2\hbar^3\omega^3} \left(1 - \frac{\Delta_{\tau s}^2}{\omega^2}\right) \left[\left(1 + \frac{\Delta_{\tau s}^2}{\omega^2}\right) \frac{(\hat{\mathbf{a}} \cdot \hat{\mathbf{b}})\hat{\mathbf{c}} \cdot \hat{\mathbf{d}} + (\hat{\mathbf{a}} \cdot \hat{\mathbf{c}})\hat{\mathbf{b}} \cdot \hat{\mathbf{d}}}{4} - \left(1 - \frac{\Delta_{\tau s}^2}{\omega^2}\right) \frac{(\hat{\mathbf{a}} \cdot \hat{\mathbf{d}})\hat{\mathbf{b}} \cdot \hat{\mathbf{c}}}{4} \right],\end{aligned}\quad (17)$$

and

$$\begin{aligned}\tilde{\xi}_{1,\tau s}^{bc}(\omega) &= \frac{\Theta(\omega - 2\Delta_{\tau s})e^2}{2\hbar^2\omega} \left[\frac{-\Delta_{\tau s}\hat{\mathbf{z}} \cdot (\hat{\mathbf{b}} \times \hat{\mathbf{c}})}{\omega} \right], \\ \tilde{\xi}_{2,\tau s}^{bcde}(\omega) &= \frac{\Theta(\omega - \Delta_{\tau s})e^4 t^2}{\hbar^4\omega^5} \left(1 - \frac{\Delta_{\tau s}^2}{\omega^2}\right) \frac{\Delta_{\tau s}}{\omega} \left[\frac{\hat{\mathbf{c}} \cdot \hat{\mathbf{e}}(\hat{\mathbf{d}} \times \hat{\mathbf{b}}) \cdot \hat{\mathbf{z}} + \hat{\mathbf{b}} \cdot \hat{\mathbf{e}}(\hat{\mathbf{d}} \times \hat{\mathbf{c}}) \cdot \hat{\mathbf{z}} + \hat{\mathbf{c}} \cdot \hat{\mathbf{d}}(\hat{\mathbf{e}} \times \hat{\mathbf{b}}) \cdot \hat{\mathbf{z}} + \hat{\mathbf{d}} \cdot \hat{\mathbf{b}}(\hat{\mathbf{e}} \times \hat{\mathbf{c}}) \cdot \hat{\mathbf{z}}}{4} \right], \\ \tilde{\eta}_{i,\tau s}^{abcd}(\omega) &= \frac{i\Theta(\omega - \Delta_{\tau s})e^4 t^2}{2\hbar^3\omega^3} \left(1 - \frac{\Delta_{\tau s}^2}{\omega^2}\right) \frac{\Delta_{\tau s}}{\omega} \left[\frac{\hat{\mathbf{a}} \cdot \hat{\mathbf{c}}(\hat{\mathbf{d}} \times \hat{\mathbf{b}}) \cdot \hat{\mathbf{z}} + \hat{\mathbf{a}} \cdot \hat{\mathbf{b}}(\hat{\mathbf{d}} \times \hat{\mathbf{c}}) \cdot \hat{\mathbf{z}}}{2} \right].\end{aligned}\quad (18)$$

The coefficients with a tilde ($\tilde{}$) are chiral and related to the Berry curvature (10), while those with a bar ($\bar{}$) are not. The expressions contain a step function, $\Theta(x) = 0, 1$ as $x <, > 0$, reflecting the energy matching conditions for the photon absorption processes, which are restricted by the band gap. Notice also that, as the frequency is increased, $\xi_{1,\tau s}^{bc}$ has a discontinuity at the frequency matching the band gap, unlike $\xi_{2,\tau s}^{bcde}$ and $\eta_{i,\tau s}^{abcd}$, which increase starting from zero at the same frequency, this is illustrated in the plots of Fig. 2. This is a general distinctive feature between one- and two-photon absorption processes, which can be seen from the optical absorption coefficients in Eq. (15); while $\Gamma_{1,cv}^{bc}$ is finite for $k = 0$ (the points in the Brillouin zone corresponding to the minimal energy excitation across the band gap), $\Gamma_{2,cv}^{bcde}$ and $\Gamma_{i,cv}^{abcd}$ vanish at $k = 0$.

The other coefficients can be obtained from these by

$$\begin{aligned}\zeta_{\tau s}(\omega) &= \hbar s \xi_{\tau s}(\omega), \\ \vartheta_{\tau s}(\omega) &= 2\tau \xi_{\tau s}(\omega), \\ \mu_{\tau s}(\omega) &= \frac{\hbar s}{2e} \eta_{\tau s}(\omega), \\ \nu_{\tau s}(\omega) &= \frac{\tau}{e} \eta_{\tau s}(\omega),\end{aligned}\quad (19)$$

where here and below we omit the indices indicating absorption process and Cartesian components. The results above are for one Dirac cone only; in order to find total injected quantities it is necessary to sum the contributions from the four Dirac cones, with the following results for the optical injection coefficients

$$\begin{aligned}\xi(\omega) &= 2[\bar{\xi}_{++}(\omega) + \bar{\xi}_{+-}(\omega)], \\ \zeta(\omega) &= 2\hbar i [\tilde{\xi}_{++}(\omega) - \tilde{\xi}_{+-}(\omega)], \\ \vartheta(\omega) &= 4i [\tilde{\xi}_{++}(\omega) + \tilde{\xi}_{+-}(\omega)],\end{aligned}\quad (20)$$

and

$$\begin{aligned}\eta(\omega) &= 2[\bar{\eta}_{++}(\omega) + \bar{\eta}_{+-}(\omega)], \\ \mu(\omega) &= \frac{\hbar i}{e} [\tilde{\eta}_{++}(\omega) - \tilde{\eta}_{+-}(\omega)], \\ \nu(\omega) &= \frac{2i}{e} [\tilde{\eta}_{++}(\omega) + \tilde{\eta}_{+-}(\omega)].\end{aligned}\quad (21)$$

We next analyze these results for different polarizations.

IV. RESULTS

For the system we are considering, one- and two-photon absorption processes inject scalar quantities while interference processes inject vectorial ones, so carriers, spin, and valley

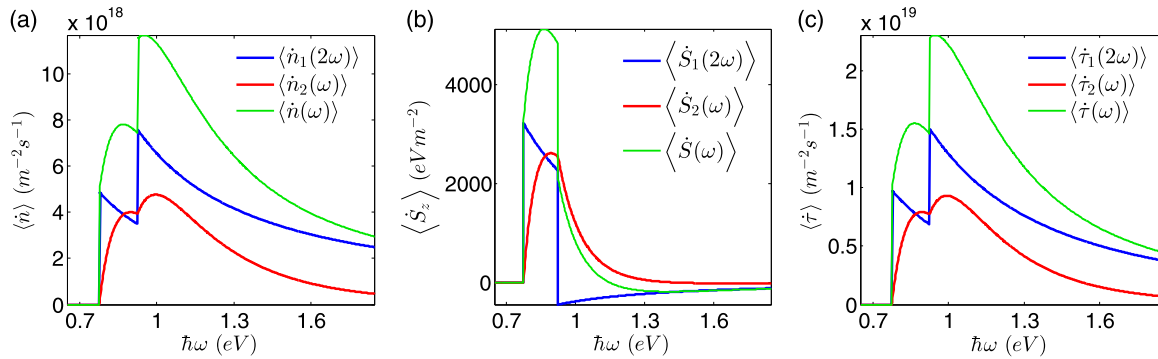


FIG. 2. (Color online) Injection rates for (a) carrier, (b) spin, and (c) valley densities. Blue lines correspond to one-photon absorption processes, red ones to two-photon processes, and green lines correspond to their sum.

densities are injected by one- and two-photon absorption processes, but not from the interference between them. Conversely, charge, spin, and valley currents are injected solely from the interference processes, not from the one- and two-photon absorption processes.

Also, the optical selection rules depend on the polarization of the incident field: while linearly polarized light couples to electrons in both valleys, circularly polarized light couples to electrons in only one valley, according to its helicity. This results in different scenarios for the injection of spin- and valley-polarized currents according to the polarization of the incident fields. Therefore we list our results below in separate subsections for different polarizations.

Finally, for any quantity considered, there will always be three distinctive frequency ranges: $\omega < \Delta_{++}$, where there is no photon absorption and no optical injection; $\Delta_{++} < \omega < \Delta_{+-}$, where there is photon absorption involving only the upper valence band, but not the lower; and $\Delta_{+-} < \omega$, where there is photon absorption involving both valence bands. The contributions of the two valence bands to the injection of spin density and spin current density have opposite signs, while their contribution to carrier and valley densities along with charge and valley current densities have equal signs. Therefore the injection of quantities associated with spin will be enhanced in the second frequency range, while the injection of quantities associated to charge and valley will be larger in the third range.

In the remainder of this section we display our results for different polarizations of the incident fields. The list of coefficients used in the expressions for the injection rates can be found in the Appendix A, while Figs. 2 and 3 contain plots of the injection rates for the quantities of interest, calculated for MoS₂ with the parameters [4] of Table I.

We consider field amplitudes of $E_\omega = 4.1 \times 10^5 \frac{V}{m}$ for the fundamental and $E_{2\omega} = 100 \frac{V}{m}$ for the second harmonic, which are indicative of the largest field intensities allowed within a simple estimate of the validity of the perturbative regime. The values chosen for E_ω and $E_{2\omega}$ differ from each other by

TABLE I. Values of the parameters used for the plots.

$\hbar t$	$\hbar \lambda$	$\hbar \Delta$	E_ω	$E_{2\omega}$
3.5 Å eV	0.15 eV	1.7 eV	$4.1 \times 10^5 \frac{V}{m}$	$100 \frac{V}{m}$

orders of magnitude because they are associated with two- and one-photon absorption processes, respectively, and since photon absorption can be treated perturbatively for the sets of frequencies and intensities considered here, it is expected that a higher-order term requires a much higher intensity to produce similar results, which is necessary for optimal interference. These values depend on the expressions for the injected carrier density, so we explain how they are obtained in Sec. V.

A. Circular polarizations

For circular polarizations $\mathbf{E}(\omega) = E_\omega e^{i\theta_1} \hat{\mathbf{p}}_{h_1}$ and $\mathbf{E}(2\omega) = E_{2\omega} e^{i\theta_2} \hat{\mathbf{p}}_{h_2}$ where $h_1, h_2 = \pm 1$ are the helicities of the light fields propagating along the \hat{z} direction, and $\hat{\mathbf{p}}_\pm = (\hat{x} \pm i\hat{y})/\sqrt{2}$, so $\hat{\mathbf{p}}_h \cdot \hat{\mathbf{p}}_h = 0$ and $\hat{\mathbf{p}}_+ \cdot \hat{\mathbf{p}}_- = 1$ as well as $\hat{\mathbf{p}}_- \times \hat{\mathbf{p}}_+ = i\hat{z}$; both E_ω and $E_{2\omega}$ are real and positive.

The injection rates for densities are given by

$$\begin{aligned} \langle \dot{n} \rangle &= \bar{\xi}_1^{-+}(2\omega) E_{2\omega}^2 + \bar{\xi}_2^{-++}(\omega) E_\omega^4, \\ \langle \dot{S}_z \rangle &= h_2 \tilde{\xi}_1^{-+}(2\omega) E_{2\omega}^2 + h_1 \tilde{\xi}_2^{-++}(\omega) E_\omega^4, \\ \langle \dot{t} \rangle &= h_2 \tilde{\nu}_1^{-+}(2\omega) E_{2\omega}^2 + h_1 \tilde{\nu}_2^{-++}(\omega) E_\omega^4. \end{aligned} \quad (22)$$

The two contributing terms, along with their final sum, are plotted in Fig. 2 for each quantity.

The one-photon injection rate has two discontinuities at $\omega = \Delta_{++}$ and $\omega = \Delta_{+-}$, as the band gaps of the Dirac cones corresponding to the two spins are reached. This is due to the Van Hove singularity of the density of states at energies matching the band gaps. The injection rates then decay for higher frequencies even though the density of states increases with the energy. This is due to the extra frequency factors in the denominator of the interaction Hamiltonian. The two-photon injection rates depend on the diagonal matrix elements of the velocity operator, which vanish at the points of the Brillouin zone with energy difference equal to the band gap. Therefore the two-photon injection rates increase continuously from zero as the frequency crosses the band gaps.

As mentioned before, circularly polarized light couples to only one valley, so the injected carriers are fully valley polarized. For $\Delta_{++} < \omega < \Delta_{+-}$, the carriers are also fully spin polarized, as only electrons from one valence band are excited. But for $\omega > \Delta_{+-}$ electrons from both valence bands are excited, and the net spin polarization is small. This is illustrated in Fig. 2. While for carriers [Fig. 2(a)], and valley polarization [Fig. 2(c)], the spikes at frequencies matching the

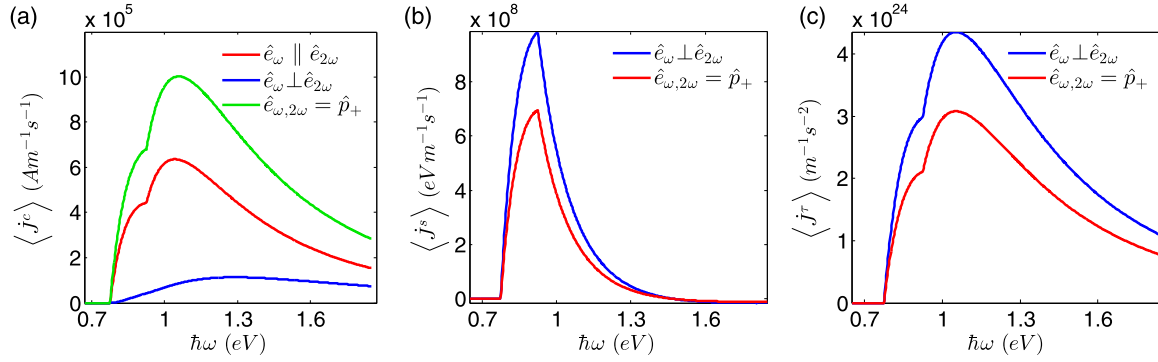


FIG. 3. (Color online) Injection rates for current densities of (a) charge, (b) spin, and (c) valley. Each line corresponds to a different choice of polarizations of the incident fields as indicated in the legends.

band gaps add constructively, for spin polarization [Fig. 2(b)], they nearly cancel out. The orientation of the spin and valley polarizations are set by the helicities of the incident fields, which determines the valley that is being coupled to the incident field.

Equal helicities. The interference process depends on the relative helicities of the two light fields, with contributions to the injected current densities only when the helicities are equal, $\mathbf{E}(\omega) = E_\omega e^{i\theta_1} \hat{\mathbf{p}}_h$ and $\mathbf{E}(2\omega) = E_{2\omega} e^{i\theta_2} \hat{\mathbf{p}}_h$.

The charge current injection rate is given by

$$\langle \mathbf{J}^c \rangle = \sqrt{2}[\hat{x} \sin(\Delta\theta) + \hat{y} \cos(\Delta\theta)]i\bar{\eta}_i^{+--+}(\omega)E_\omega^2 E_{2\omega}, \quad (23)$$

where $\Delta\theta = \theta_2 - 2\theta_1$ is the relative phase parameter, and the injection rates for spin and valley currents are

$$\begin{aligned} \langle \mathbf{J}^s \rangle &= \sqrt{2}h[\hat{x} \sin(\Delta\theta) + \hat{y} \cos(\Delta\theta)]i\tilde{\mu}_i^{+--+}(\omega)E_\omega^2 E_{2\omega}, \\ \langle \mathbf{J}^v \rangle &= \sqrt{2}h[\hat{x} \sin(\Delta\theta) + \hat{y} \cos(\Delta\theta)]i\tilde{\nu}_i^{+--+}(\omega)E_\omega^2 E_{2\omega}. \end{aligned} \quad (24)$$

These expressions are illustrated in Fig. 3. The currents do not increase sharply as the band gaps are reached because the velocity of carriers at the bottom of the conduction bands vanish.

The injected current densities of spin and valley are due to the fact that the carriers are polarized, and have the same characteristics as the injected charge current density. As discussed for the injection of the spin density, the spin polarization is greatly diminished for higher frequencies, and the injected spin current density also follows this trend as shown in Fig. 3(b).

All the currents are injected along the same direction, which can be controlled by the relative phase between the light fields. The spin and valley density injection rates depend directly on the Berry curvature (10), while the carrier density injection is independent of it. The orientation of the spin and valley currents are set by the helicity of the incident fields, which has to match the chirality of the Dirac cone.

Opposite helicities. When the light fields have different helicities, the injection rates from interference vanish for all the current densities of interest.

B. Linear polarizations

The one- and two-photon injection processes do not depend on the relative orientation of the fundamental $\mathbf{E}(\omega) =$

$E_\omega e^{i\theta_1} \hat{\mathbf{e}}_\omega$ and second harmonic $\mathbf{E}(2\omega) = E_{2\omega} e^{i\theta_2} \hat{\mathbf{e}}_{2\omega}$ fields, where E_ω and $E_{2\omega} > 0$ are real, as are $\hat{\mathbf{e}}_\omega$ and $\hat{\mathbf{e}}_{2\omega}$. Therefore we show here the results for the injection coefficients Λ_1 and Λ_2 , while the results for Λ_i are displayed for the special cases of parallel and perpendicular polarizations.

The carrier density injection rate is given by

$$\langle \dot{n} \rangle = \bar{\xi}_1^{xx}(2\omega)E_{2\omega}^2 + \bar{\xi}_2^{xxxx}(\omega)E_\omega^4. \quad (25)$$

When plotted as a function of frequency, the two contributing terms, along with the final sum, have a shape similar to the corresponding curves for circular polarizations, which are plotted in Fig. 2(a).

Linearly polarized light couples to both valleys, which results in an injected carrier density only. It neither injects spin- nor valley-polarization densities, because the contributions to these quantities from the two valleys cancel each other.

The one- and two-photon injection rates of the current densities vanish $\langle \mathbf{J}_1^{c,s,\tau} \rangle = \langle \mathbf{J}_2^{c,s,\tau} \rangle = 0$. These currents are injected only through the interference process, and we discuss the results for \mathbf{J} for different polarization orientations of the incident light below $\langle \mathbf{J}_i^{c,s,\tau} \rangle$.

Parallel orientations. Only the interference process depends on the relative orientation of $\mathbf{E}(\omega) = E_\omega e^{i\theta_1} \hat{\mathbf{e}}_\omega$ and $\mathbf{E}(2\omega) = E_{2\omega} e^{i\theta_2} \hat{\mathbf{e}}_\omega$.

The charge current density injection rate is given by

$$\langle \mathbf{J}^c \rangle = 2\hat{e}_\omega i\bar{\eta}_i^{xxxx}(\omega) \sin(\Delta\theta)E_\omega^2 E_{2\omega}, \quad (26)$$

which is plotted in Fig. 3(a); the relative phase parameter is again $\Delta\theta = \theta_2 - 2\theta_1$. It increases from zero once excitations from the higher valence band are possible ($\omega > \Delta_{++}$), and has a second contribution for excitations from the lower valence band at higher frequencies ($\omega > \Delta_{+-}$).

When the incident fields are linearly polarized in the same direction, the excited carriers move in the same direction in both valleys, which corresponds to a charge current that is neither spin nor valley polarized.

The direction of the polarization vector provides control of the angle of the injected charge current, while the relative phase parameter of the light beams can control only their magnitude and orientation.

Perpendicular orientations. Here we have $\mathbf{E}(\omega) = E_\omega e^{i\theta_1} \hat{\mathbf{e}}_\omega$ and $\mathbf{E}(2\omega) = E_{2\omega} e^{i\theta_2} \hat{\mathbf{e}}_{2\omega}$, and we take $\hat{\mathbf{e}}_{2\omega} = \hat{z} \times \hat{\mathbf{e}}_\omega$. The relative phase parameter is again $\Delta\theta = \theta_2 - 2\theta_1$.

The charge current injection rate is given by

$$\langle \dot{\mathbf{J}}^c \rangle = 2\hat{e}_{2\omega} i \bar{\eta}_i^{xyxy}(\omega) \sin(\Delta\theta) E_\omega^2 E_{2\omega}, \quad (27)$$

where $\Delta\theta = \theta_2 - 2\theta_1$ is the relative phase parameter, and the injection rates for spin and valley current densities are

$$\begin{aligned} \langle \dot{\mathbf{J}}^s \rangle &= 2\hat{e}_\omega \bar{\mu}_i^{xyxy}(\omega) \cos(\Delta\theta) E_\omega^2 E_{2\omega}, \\ \langle \dot{\mathbf{J}}^\tau \rangle &= 2\hat{e}_\omega \bar{v}_i^{xyxy}(\omega) \cos(\Delta\theta) E_\omega^2 E_{2\omega}, \end{aligned} \quad (28)$$

which are plotted in Fig. 3. Again the spin polarization is greatly suppressed for higher frequencies ($\omega > \Delta_{+-}$), because the valence bands in each valley have opposite spin.

When the incident fields are linearly polarized in perpendicular directions, the contributions from the two valleys are combined according to the phase parameter $\Delta\theta$. Therefore, for some values of $\Delta\theta$, the carriers in both valleys will move in the same direction, which amounts to a charge current and no spin or valley currents. For other values of $\Delta\theta$, the carriers in different valleys will have opposite direction, which leads to no charge current density, but finite spin and valley current densities.

The control scenario here is unique: the charge current is injected along the direction of the second harmonic field, while the spin and valley currents are injected along the direction of the fundamental field. The relative phase parameter $\Delta\theta$ can control their magnitude, with the remarkable ability to switch between charge current or spin and valley currents perpendicular to it.

V. DISCUSSION

The validity of our calculations for the optical injection rates depends on the validity of the perturbative regime, which requires that the fraction of the injected carrier population relative to the total number of states in the range of energies covered by the laser pulse be small [23]. The duration of the pulse \mathcal{T} sets the frequency broadening of the laser $\Delta\omega = \frac{2\pi}{\mathcal{T}}$, which in turn—via the dispersion relation—determines the area a of the Brillouin zone that can be populated by carriers, $a = 2\pi k \Delta k$. The momentum width Δk is set by the dispersion relation and is proportional to $\Delta\omega$. The number of states available in this area of the Brillouin zone is a/a_1 , where $a_1 = \frac{(2\pi)^2}{L^2}$ is the area occupied by one state. If we restrict the maximum amplitudes of the laser fields by the condition that the number of injected carriers with additional energy $2\hbar\omega$ is at most 5% of the total number of carrier states in the allowed energy range, we require

$$(\bar{\xi}_1^{-+}(2\omega)E_{2\omega}^2 + \bar{\xi}_2^{-++}(\omega)E_\omega^4)\mathcal{T}L^2 < 0.05 \frac{a}{a_1}. \quad (29)$$

We then estimate the amplitudes by imposing the additional condition $\bar{\xi}_1^{-+}(2\omega)E_{2\omega}^2 = \bar{\xi}_2^{-++}(\omega)E_\omega^4$, which gives optimal interference between the absorption processes [14]. For pulses lasting $1ns$ with a frequency corresponding to $\hbar\omega = 0.9eV$, the field amplitudes found are $E_\omega = 4.1 \cdot 10^5 \frac{V}{m}$ for the fundamental and $E_{2\omega} = 100 \frac{V}{m}$ for the second harmonic, which correspond to laser intensities of $22 \frac{kW}{cm^2}$ and $1.3 \frac{mW}{cm^2}$,

respectively. As mentioned before, the values of E_ω and $E_{2\omega}$ corresponding to optimal interference differ from each other by orders of magnitude because they are associated with two- and one-photon absorption processes respectively, and in the perturbative analysis, it is expected that a higher-order term requires a much higher intensity to produce similar results. We use the above values of E_ω and $E_{2\omega}$ for all $\hbar\omega$ in Figs. 2 and 3, despite the fact that with these values (29) is only satisfied for $\hbar\omega \geq 0.9eV$; but of course the violation is not too large for frequencies $\hbar\omega \sim 0.8eV$. Equation (29) can be used to determine the appropriate field amplitudes for other frequencies and time duration of the laser pulses. Relaxation of the injected carriers was not included in the estimation of the validity of the perturbative regime. If it were included it would reduce any Pauli blocking, and hence lead to the prediction that larger pulse intensities or durations could still be treated perturbatively.

Although the detection of the spin- or valley-polarized current is difficult, it can be done by pump-probe experiments [24,25] with circularly polarized light. This would allow for measuring the separation between the two components of spin or valley after the current is injected. Experiments using an analogous technique have already been performed for monolayer TMDs [26,27].

Corrections to the injection rate coefficients due to the electron-hole interaction lead to a shift δ in the phase parameter $\Delta\theta$, which becomes $\Delta\theta = \theta_2 - 2\theta_1 + \delta$. For semiconductors, this shift is too small to be easily detected [28]. However, since calculations for exciton binding energies [29] indicate that monolayer TMDs have a stronger electron-hole interaction, it is reasonable to expect a considerable shift δ for them. This phase shift can be measured by simply varying the relative phases of the incident fields, and measuring the phases that lead to the maximum injection rates since they are proportional to either $\sin(\Delta\theta)$ or $\cos(\Delta\theta)$. Hence the experiments we are suggesting here could serve as a probe of the electron-hole interactions in these materials.

VI. CONCLUSION

We perturbatively computed the optical injection rates of charge, spin, and valley densities and currents in monolayer TMDs, for an incident optical field in addition to its second harmonic. We verified that the interference of one- and two-photon absorption processes allows for the injection of currents, resulting in an all-optical method for current injection that can be fast switched. We also discussed how the relative phase parameter between the two incident fields, as well as their polarization, can be used to control the injected currents, allowing for a more refined analysis than the ones obtained with DC fields. Additionally, we estimated the validity of our calculations and discussed the prospects of experimental verification of our results.

Finally, we emphasize the advantage of the all-optical method in studying and controlling the injected currents. In all-optical injection the carriers are injected in specific locations of the Brillouin zone, while static fields only slightly unbalance the distribution of carriers. This difference can be used to study the scattering rate of carriers in specific regions of the Brillouin zone in a direct way. It can be also used for more refined control

of the injected quantities. The results of our calculations show that it is possible to control the direction and intensity of the injected currents by simply changing the relative phase of the fields, which can be achieved in a time scale limited only by the duration of the pulses used. This is perhaps more dramatic when the perpendicular linear polarizations are considered. In this case, the phase parameter $\Delta\theta$ allows us to select between charge currents or perpendicular spin and valley currents. A similar effect usually occurs when DC fields are used for photocurrent injection [3], where a charge current is converted into perpendicular spin and valley currents, due to the opposite Berry curvature in the two valleys. But in that process it is not possible to control the currents, or fast switch between the two cases, in contrast to the all-optical method considered in this paper. We therefore expect that our results will be helpful for understanding the details of these promising materials, and clarifying their potential to implement ultrafast optical switching.

ACKNOWLEDGMENTS

We thank Andor Kormanyos and Jin-Luo Cheng for helpful discussions. This work was supported by the Natural Sciences and Engineering Research Council of Canada (NSERC).

APPENDIX: OPTICAL INJECTION COEFFICIENTS FOR LINEAR AND CIRCULAR POLARIZATIONS

The coefficients used for one- and two-photon absorption processes, obtained from Eq. (14), are

$$\begin{aligned}\bar{\xi}_{1,\tau s}^{xx}(\omega) &= \frac{\Theta(\omega - 2\Delta_{\tau s})e^2}{8\hbar^2\omega} \left(1 + \frac{4\Delta_{\tau s}^2}{\omega^2}\right), \\ \bar{\xi}_{2,\tau s}^{xxxx}(\omega) &= \frac{\Theta(\omega - \Delta_{\tau s})e^4 t^2}{4\hbar^4\omega^5} \left(1 - \frac{\Delta_{\tau s}^2}{\omega^2}\right) \left(1 + \frac{3\Delta_{\tau s}^2}{\omega^2}\right),\end{aligned}\quad (A1)$$

and for linear polarization.

For circular polarization we have

$$\begin{aligned}\bar{\xi}_{1,\tau s}^{-+}(\omega) &= \frac{\Theta(\omega - 2\Delta_{\tau s})e^2}{8\hbar^2\omega} \left(1 + \frac{4\Delta_{\tau s}^2}{\omega^2}\right), \\ \bar{\xi}_{2,\tau s}^{-++}(\omega) &= \frac{\Theta(\omega - \Delta_{\tau s})e^4 t^2}{2\hbar^4\omega^5} \left(1 - \frac{\Delta_{\tau s}^2}{\omega^2}\right) \left(1 + \frac{\Delta_{\tau s}^2}{\omega^2}\right),\end{aligned}\quad (A2)$$

and

$$\begin{aligned}\tilde{\xi}_{1,\tau s}^{-+}(\omega) &= \frac{-i\Theta(\omega - 2\Delta_{\tau s})e^2}{2\hbar^2\omega} \left(\frac{\Delta_{\tau s}}{\omega}\right), \\ \tilde{\xi}_{2,\tau s}^{-++}(\omega) &= \frac{-i\Theta(\omega - \Delta_{\tau s})e^4 t^2}{\hbar^4\omega^5} \left(1 - \frac{\Delta_{\tau s}^2}{\omega^2}\right) \frac{\Delta_{\tau s}}{\omega}.\end{aligned}\quad (A3)$$

The interference coefficients for linear polarizations are

$$\begin{aligned}\bar{\eta}_{i,\tau s}^{xxxx}(\omega) &= \frac{i\Theta(\omega - \Delta_{\tau s})e^4 t^2}{8\hbar^3\omega^3} \left(1 - \frac{\Delta_{\tau s}^2}{\omega^2}\right) \left(1 + \frac{3\Delta_{\tau s}^2}{\omega^2}\right), \\ \bar{\eta}_{i,\tau s}^{yyxy}(\omega) &= \frac{-i\Theta(\omega - \Delta_{\tau s})e^4 t^2}{8\hbar^3\omega^3} \left(1 - \frac{\Delta_{\tau s}^2}{\omega^2}\right)^2\end{aligned}\quad (A4)$$

and

$$\tilde{\eta}_{i,\tau s}^{xyxy}(\omega) = \frac{-i\Theta(\omega - \Delta_{\tau s})e^4 t^2}{2\hbar^3\omega^3} \left(1 - \frac{\Delta_{\tau s}^2}{\omega^2}\right) \frac{\Delta_{\tau s}}{\omega},\quad (A5)$$

while for circular polarizations the coefficients are

$$\begin{aligned}\bar{\eta}_{i,\tau s}^{+--+}(\omega) &= \frac{i\Theta(\omega - \Delta_{\tau s})e^4 t^2}{4\hbar^3\omega^3} \left(1 - \frac{\Delta_{\tau s}^2}{\omega^2}\right) \left(1 + \frac{\Delta_{\tau s}^2}{\omega^2}\right), \\ \tilde{\eta}_{i,\tau s}^{+--+}(\omega) &= \frac{\Theta(\omega - \Delta_{\tau s})e^4 t^2}{2\hbar^3\omega^3} \left(1 - \frac{\Delta_{\tau s}^2}{\omega^2}\right) \frac{\Delta_{\tau s}}{\omega}.\end{aligned}\quad (A6)$$

The other injection rate coefficients are obtained from the ones above.

-
- [1] S. Z. Butler, S. M. Hollen, L. Cao, Y. Cui, J. A. Gupta, H. R. Gutierrez, T. F. Heinz, S. S. Hong, J. Huang, A. F. Ismach, E. Johnston-Halperin, M. Kuno, V. V. Plashnitsa, R. D. Robinson, R. S. Ruoff, S. Salahuddin, J. Shan, L. Shi, M. G. Spencer, M. Terrones, W. Windl, and J. E. Goldberger, *ACS Nano* **7**, 2898 (2013).
- [2] Qing Hua Wang, Kourosh Kalantar-Zadeh, Andras Kis, Jonathan N. Coleman, and Michael S. Strano, *Nature Nanotechnol.* **7**, 699 (2012).
- [3] Xiaodong Xu, Wang Yao, Di Xiao, and Tony F. Heinz, *Nature Phys.* **10**, 343 (2014).
- [4] Di Xiao, Gui-Bin Liu, Wanxiang Feng, Xiaodong Xu, and Wang Yao, *Phys. Rev. Lett.* **108**, 196802 (2012).
- [5] Habib Rostami, Ali G. Moghaddam, and Reza Asgari, *Phys. Rev. B* **88**, 085440 (2013).
- [6] Zhou Li, and J. P. Carbotte, *Phys. Rev. B* **86**, 205425 (2012).
- [7] Felix Rose, M. O. Goerbig, and Frederic Piechon, *Phys. Rev. B* **88**, 125438 (2013).
- [8] Xiao Li, Fan Zhang, and Qian Niu, *Phys. Rev. Lett.* **110**, 066803 (2013).
- [9] Aaron M. Jones, Hongyi Yu, Nirmal J. Ghimire, Sanfeng Wu, Grant Aivazian, Jason S. Ross, Bo Zhao, Jiaqiang Yan, David G. Mandrus, Di Xiao, Wang Yao, and Xiaodong Xu, *Nature Nanotechnol.* **8**, 634 (2013).
- [10] Kin Fai Mak, Keliang He, Jie Shan, and Tony F. Heinz, *Nature Nanotechnol.* **7**, 494 (2012).
- [11] Hualing Zeng, Junfeng Dai, Wang Yao, Di Xiao, and Xiaodong Cui, *Nature Nanotechnol.* **7**, 490 (2012).
- [12] Nardeep Kumar, Sina Najmaei, Qiannan Cui, Frank Ceballos, Pulickel M. Ajayan, Jun Lou, and Hui Zhao, *Phys. Rev. B* **87**, 161403(R) (2013).

- [13] L. M. Malard, T. V. Alencar, Ana Paula M. Barboza, K. F. Mak, and A. M. de Paula, *Phys. Rev. B* **87**, 201401(R) (2013).
- [14] J. Rioux and J. E. Sipe, *Physica E* **45**, 1 (2012).
- [15] I. Rumyantsev and J. E. Sipe, *Phys. Rev. B* **73**, 201302(R) (2006).
- [16] D. E. Reiter, E. Ya. Sherman, A. Najmaie, and J. E. Sipe, *Europhys. Lett.* **88**, 67005 (2009).
- [17] J. Rioux and J. E. Sipe, *Phys. Rev. B* **81**, 155215 (2010).
- [18] K. M. Rao and J. E. Sipe, *Phys. Rev. B* **84**, 205313 (2011).
- [19] K. S. Virk and J. E. Sipe, *Phys. Rev. Lett.* **107**, 120403 (2011).
- [20] D. Sun, C. Divin, J. Rioux, J. E. Sipe, C. Berger, W. A. de Heer, P. N. First, and T. B. Norris, *Nano Lett.* **10**, 1293 (2010).
- [21] J. Rioux, G. Burkard, and J. E. Sipe, *Phys. Rev. B* **83**, 195406 (2011).
- [22] K. M. Rao and J. E. Sipe, *Phys. Rev. B* **86**, 115427 (2012).
- [23] Rodrigo A. Muniz and J. E. Sipe, *Phys. Rev. B* **89**, 205113 (2014).
- [24] H. Zhao, E. J. Loren, H. M. van Driel, and A. L. Smirl, *Phys. Rev. Lett.* **96**, 246601 (2006).
- [25] E. Ya. Sherman, A. Najmaie, H. M. van Driel, A. L. Smirl, and J. E. Sipe, *Solid State Commun.* **139**, 439 (2006).
- [26] G. Sallen, L. Bouet, X. Marie, G. Wang, C. R. Zhu, W. P. Han, Y. Lu, P. H. Tan, T. Amand, B. L. Liu, and B. Urbaszek, *Phys. Rev. B* **86**, 081301(R) (2012).
- [27] Yang Song and Hanan Dery, *Phys. Rev. Lett.* **111**, 026601 (2013).
- [28] R. D. R. Bhat and J. E. Sipe, *Phys. Rev. B* **72**, 075205 (2005).
- [29] Diana Y. Qiu, Felipe H. da Jornada, and Steven G. Louie, *Phys. Rev. Lett.* **111**, 216805 (2013).